8-2011

Chaotic Bandgaps in Hybrid Acousto-optic Feedback and their Implications

Monish Ranjan Chatterjee
University of Dayton, mchatterjee1@udayton.edu

Mohammed A. Al-Saedi
University of Dayton

Chaotic bandgaps in hybrid acousto-optic feedback and their implications

Monish R. Chatterjee [1*] and Mohammed A. Al-Saedi [1]

[1]University of Dayton, Dept. of ECE, 300 College Park, Dayton, OH 45469-0232

*corresponding author

Email: monish.chatterjee@notes.udayton.edu

ABSTRACT

The nonlinear dynamics of a hybrid acousto-optic device was examined from the perspective of the Lyapunov exponent (LE) and bifurcation maps. The plots for LE versus system parameters and bifurcation maps have recently been examined against known simulation results including chaotic encryption experiments [1]. It is verified that the "loop gain" (feedback gain (β) times incident light amplitude (I_{in}) needs to be greater than one as a *necessary*, but not *sufficient* condition for the onset of chaos. It is found that for certain combinations of β, I_{in}, net bias voltage (α_{tot}), and the initial value of the first-order scattered light ($I_1(0)$), there are pronounced regions of chaos in the parameter field, while for others, chaos is minimal. It is also observed that in some cases, the negative "spikes" in the LE are far larger than its positive amplitudes, hence indicating a greater tendency to become non-chaotic. Additionally, we have examined the bifurcation plots versus the two most salient system parameters, α_{tot} and β. These maps have revealed behavior that is by no means uniformly chaotic. It is found that the system moves in and out of chaos within distinct *bands* along the α_{tot} and β axes. These results imply strong sensitivity vis-à-vis these parameters around the *passbands* and *stopbands*, and may indicate control of chaos by appropriate parameter adjustment. Such control may have applications in biological chaos, such as arresting malignant, chaotic cell multiplication. Overall, the dynamical results compare favorably with time-domain characteristics of encrypted chaotic waveforms in signal modulation and transmission applications.

Keywords: Acousto-optics, chaos, feedback, encryption, Lyapunov exponent, bifurcation maps, nonlinear dynamics, passbands, stopbands

1. INTRODUCTION AND BACKGROUND

Acousto-optic (A-O) bistability and chaos were first reported around the late 1970s by Albert et. al [1], when it was shown that A-O devices with positive feedback gain exhibited bistability characteristics [2]. In a standard setup, a Bragg cell is driven by an ultrasonic sound wave from an RF generator (typically at 40 MHz or higher), and the resulting sound grating diffracts an incident laser beam into the first-order under Bragg condition. The first-order is then picked up by a linear photodetector, fed to an amplifier, and then returned to the bias input of the RF generator. The arrangement is shown in Fig.1. Nominally, the scattered light beam is intrinsically frequency or phase modulated (with the acoustic frequency). In typical waveform sources, the external bias input amplitude modulates the RF waveform. A plot of the first order intensity (I_1) vs. the bias input $\hat{\alpha}_0$ yields the well known bistable and hysteretic behavior [2,3]. It is well known that when the feedback gain, or a combination of parameters is increased or adjusted sufficiently, the feedback system enters into chaos. The bistability, hysteresis and chaotic characteristics depend strongly on the feedback gain ($\tilde{\beta}$), the feedback time delay (TD), the amplitude (I_{inc}) of the incident light, the initial value of the intensity ($I_1(0)$) and the effective bias voltage ($\hat{\alpha}_0$). Using the chaotic properties of the hybrid acousto-optic feedback device (HAOF), it was recently reported that it is possible to *encrypt* relatively low bandwidth signals within the chaos

Free-Space and Atmospheric Laser Communications XI, edited by
Arun K. Majumdar, Christopher C. Davis, Proc. of SPIE Vol. 8162, 81620J
© 2011 SPIE · CCC code: 0277-786X/11/$18 · doi: 10.1117/12.890324

wave, and subsequently transmit, receive, heterodyne, filter and recover the message signal from this chaotically encrypted carrier [4,5]. This earlier work showed a reliable and relatively robust means of secure information communication for a few simple test signals applied through the acoustic bias input. While the transmitted chaotic waves appeared to have been reasonably recovered in the test simulations, the choice of input amplitudes, frequencies, and the values of the important system parameters was based in that work primarily on studying multiple simulations, and conducting the tests for conditions where chaos would appear to be fairly assured. In this paper, we examine the chaos and encryption problem from an analytic perspective, in order to be able to better understand and predict the system behavior relative to the critical parameter thresholds that are inherent in the HAOF device. In the process, we show how chaos depends critically on the combination of the four principal parameters of the closed-loop system, viz., feedback gain ($\tilde{\beta}$), the feedback time delay (TD), the amplitude (I_{inc}) of the incident light, the initial value of the intensity ($I_1(0)$) and the effective bias voltage ($\hat{\alpha}_0$). Moreover, we find that the emergence of chaos even with the right choice of parameters is not uniformly ensured over variations of one of the free parameters, i.e., $\tilde{\beta}$ and $\hat{\alpha}_0$. Within observed parameter ranges that generally ensure chaos within the nonlinear dynamics, it is found that the system is chaotic only over specific windows, herein termed chaotic passbands, and non-chaotic over other windows, termed chaotic stopbands. We present here examples of such passbands and stopbands, and their implications for signal encryption and recovery in the domain of secure communications.

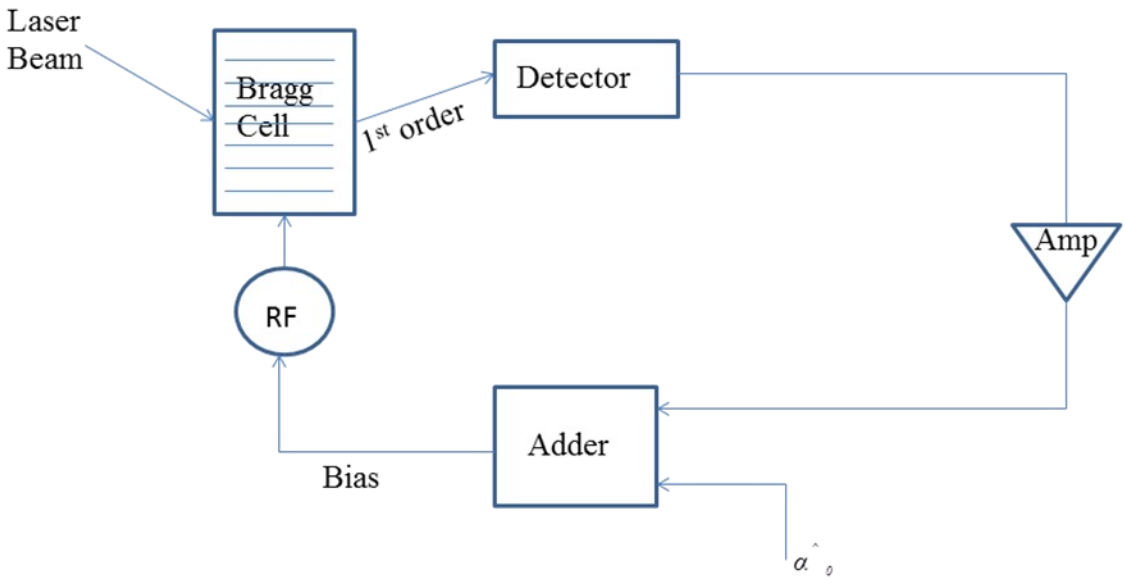

Fig. 1. The acousto-optic modulator with feedback showing Bragg cell, photodetector, amplifier and acoustic driver with composite bias input.

1.1 Analysis of chaotic behavior via the theory of Lyapunov exponents

Assuming that the sound pressure remains constant during the interaction (this enables the formation of a periodic grating within the interaction region), and the interaction time is much smaller than the feedback delay time, the intensity $I_1(n)$ of the first-order diffracted beam at the time $t = n\tau$ in a HAOF system may be described as a nonlinear one-dimensional iterative process [3,6]:

$$I_1(n) = I_{inc} \sin^2\left[\hat{\alpha}_0 + \tilde{\beta} I_1(n-1)\right] \quad , \tag{1}$$

where $\tilde{\beta}$ is the net feedback gain, I_{inc} is the intensity of the incident light beam, τ is the time delay in the feedback loop, and $n = 1, 2, 3, \ldots$ represents the number of iterations in the feedback loop. Note that Eq.(1) is the fundamental equation used in our analytical as well as simulation/numerical studies. We assume that the parameters $\hat{\alpha}_0$ and $\tilde{\beta}$ are real,

nonnegative numbers. Using standard arguments based on the development of the Lyapunov exponent, it can be shown that a *necessary*, though not *sufficient* condition in order to ensure chaos is given by [6]:

$$\left| \tilde{\beta} I_{inc} \right| > 1 , \tag{2}$$

i.e., the product of the feedback gain and the incident optical amplitude must exceed 1 in magnitude. Our numerical and analytic studies will reveal further details on this requirement.

In what follows, we examine the AO feedback problem in terms of its dynamical behavior, specifically by looking at the LE versus appropriate system parameters (with the other parameters held constant). This will be followed by a study of the bifurcation graphs of the problem (first-order intensity versus feedback gain with other parameters held constant), and rigorously verifying the resulting chaotic and non-chaotic regimes against the aforementioned Lyapunov theory. In the final analysis, we look further at the graphical results and test the outcomes against the cases for low-frequency and low-amplitude (ac) chaotic modulation simulations that have been recently reported in the context of chaotic encryption and decryption of narrowband signals [5].

1.2 Examination of dynamical behavior in light of the Lyapunov exponent

As mentioned, in this section we investigate the Lyapunov exponent (LE) defined by eq. (6.10) via 2-D plots of LE versus $\tilde{\beta}$ and $\hat{\alpha}_0$. As seen from Fig.2, in this case, $I_{inc} = I_1(0) = 0.55$, and $\hat{\alpha}_0 = 2$. We find in this case that the system is non-chaotic until the value of $\tilde{\beta} = 3.5$ is reached. Thereafter, there are "bands" of $\tilde{\beta}$ over which the LE is positive, implying chaos. We observe further that even past $\tilde{\beta} = 3.5$, there are isolated indentations in the LE values where the exponent becomes negative, implying that the system comes out of chaos.

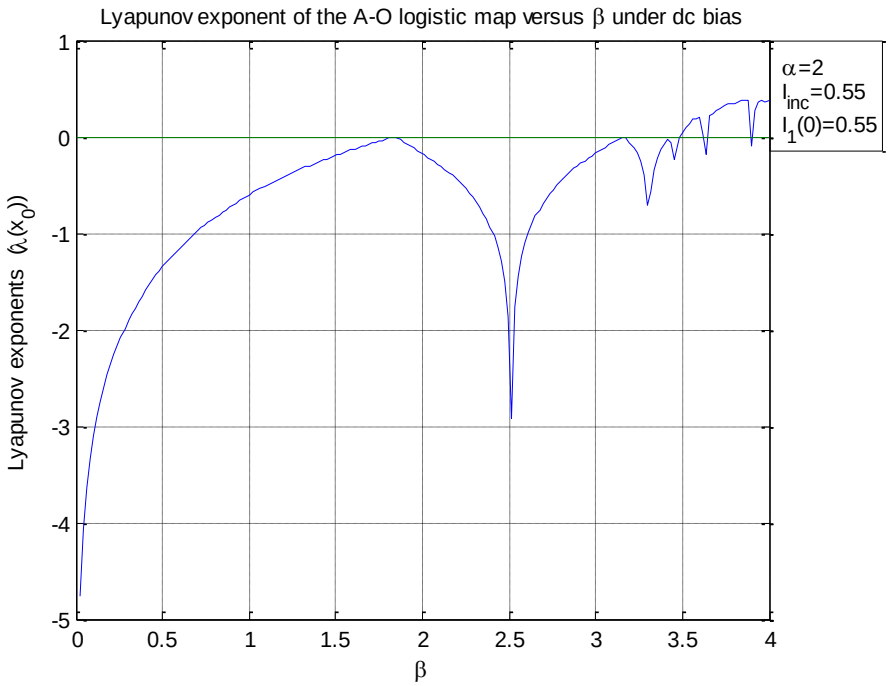

Fig.2. LE versus $\tilde{\beta}$ for $I_{inc} = I_1(0) = 0.55$ and $\hat{\alpha}_0 = 2$.

In Fig.3, the chosen values were I_{inc} = 1, $I_1(0)$ = 0, and $\hat{\alpha}_0$ = 1. In this case, we find that the LE begins to go positive at lower values of $\tilde{\beta}$ (three distinct areas around 2.4), followed by larger positive values around 3.1 and upto about 3.7, with one notable indentation. These positive areas clearly represent chaotic behavior. In the plot shown in Fig.4, we find that for I_{inc} = 1, $I_1(0)$ = 1 and $\hat{\alpha}_0$ = 2, there are two relatively broad regions of chaos, viz., a band extending from about 1.9 – 2.7, and a second one from 3.2 – 4. Within these "passbands", we again see occasional negative indentations in the LE.

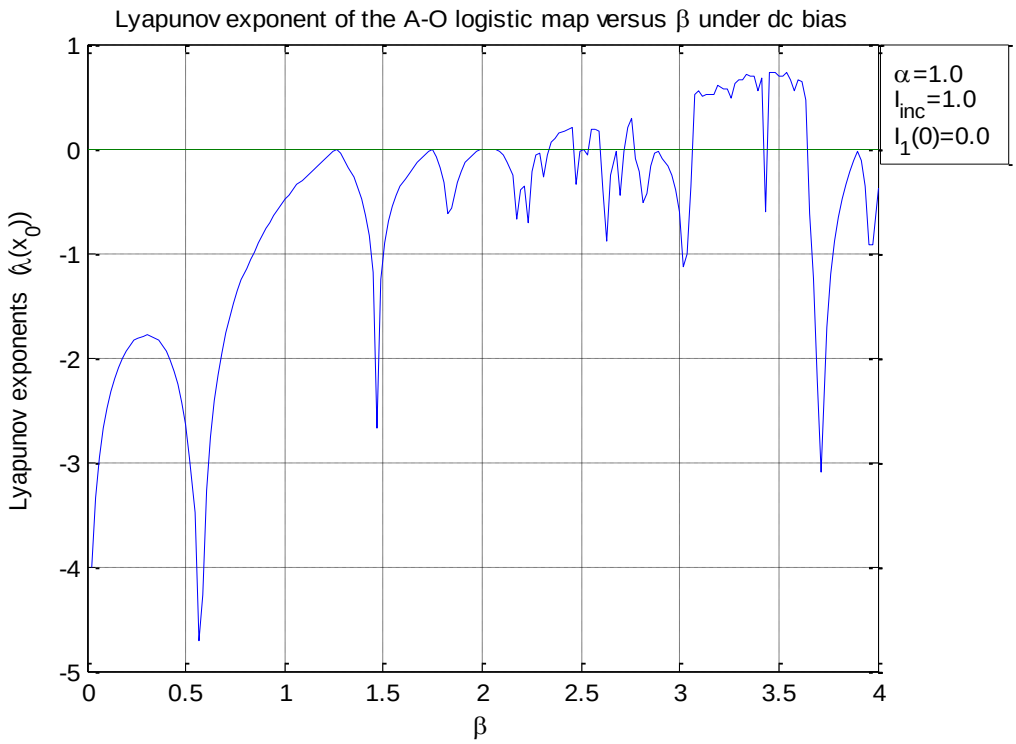

Fig.3. LE versus $\tilde{\beta}$ for I_{inc} = 1.0, I_1 (0) = 0.0 and $\hat{\alpha}_0$ = 1.

In studying the feedback characteristics due to the LE, it turns out that examining the exponent relative to the acoustic driver bias ($\hat{\alpha}_0$) is more crucial to the implementation of signal modulation and encryption operations than LE versus $\tilde{\beta}$. This is because the (ac) signal input for the encryption operations invariably goes through the acoustic driver, and hence influences the $\hat{\alpha}_0$ behavior. We next illustrate our LE versus $\hat{\alpha}_0$ characteristics indicating some differences vis-a-vis the corresponding dependence on $\tilde{\beta}$. In Fig.5, the chosen parameters are: I_{inc} = 1, $I_1(0)$ = 2, and $\tilde{\beta}$ = 2. From the figure, we find that for the chosen values, LE becomes positive over relatively small "bands" of $\hat{\alpha}_0$, while over much wider swaths of $\hat{\alpha}_0$, LE assumes negative values (including regions where it is highly negative). Overall, this would indicate that for these parameters, the system is chaotic only over a rather limited choice of $\hat{\alpha}_0$ values (such as around 0.7 and 1.85).

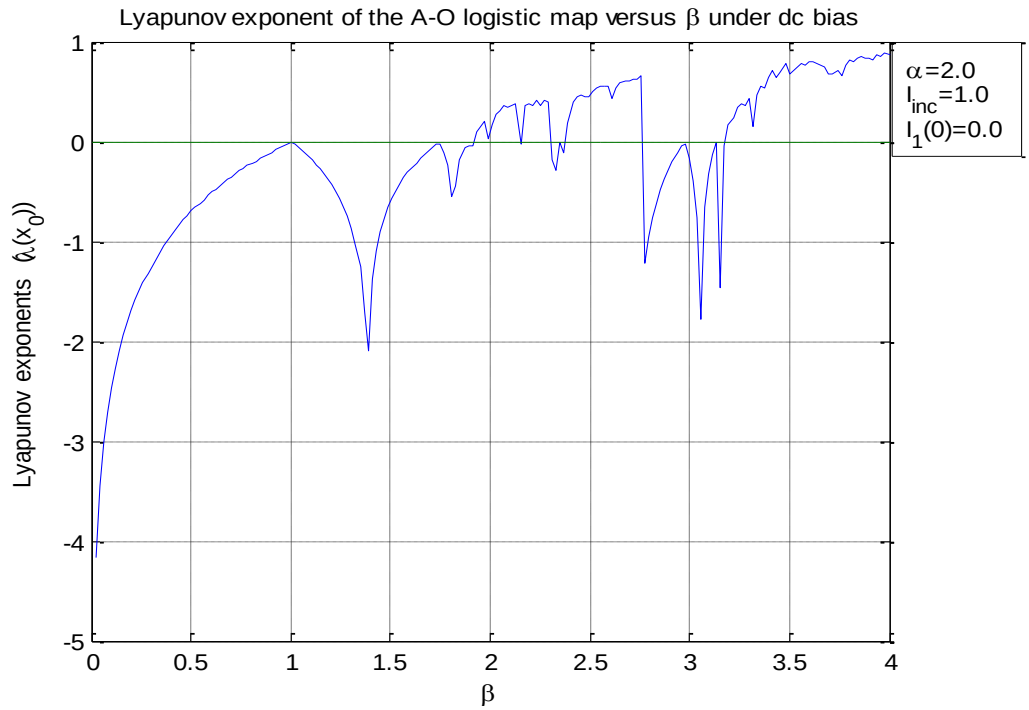

Fig.4. LE versus $\tilde{\beta}$ for $I_{inc} = 1$, $I_1(0) = 0$, and $\hat{\alpha}_0 = 2$.

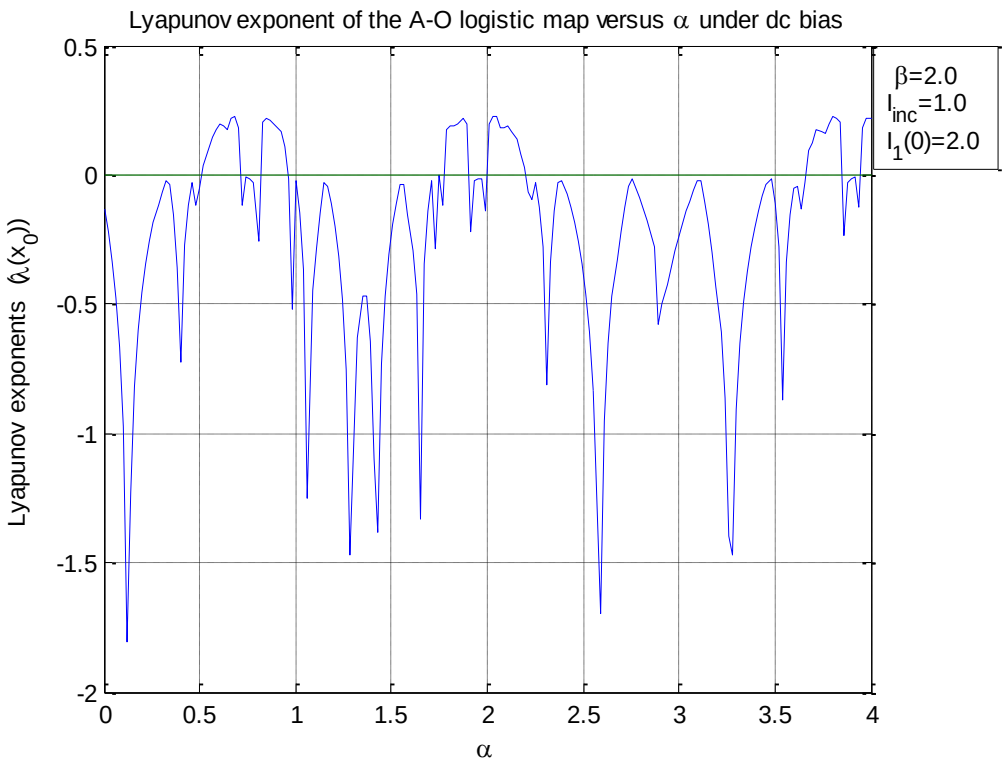

Fig.5. LE versus $\hat{\alpha}_0$ for $I_{inc} = 1$, $I_1(0) = 2$, and $\tilde{\beta} = 2$.

The parameters corresponding to Fig.6, on the other hand, are: $I_{inc} = 1$, $I_1(0) = 0$ and $\tilde{\beta} = 2$. We note here that with $I_{inc} = 1$ and $I_1(0) = 0$, there are only very limited bands in the $\hat{\alpha}_0$ space where chaos happens when $\tilde{\beta} = 2$. This finding is in complete agreement with our reported modulation results where it was seen that with $I_{inc} = 1$ and $I_1(0) = 0$, chaos occurs only when $\tilde{\beta}$ exceeds 2.41 [5,7].

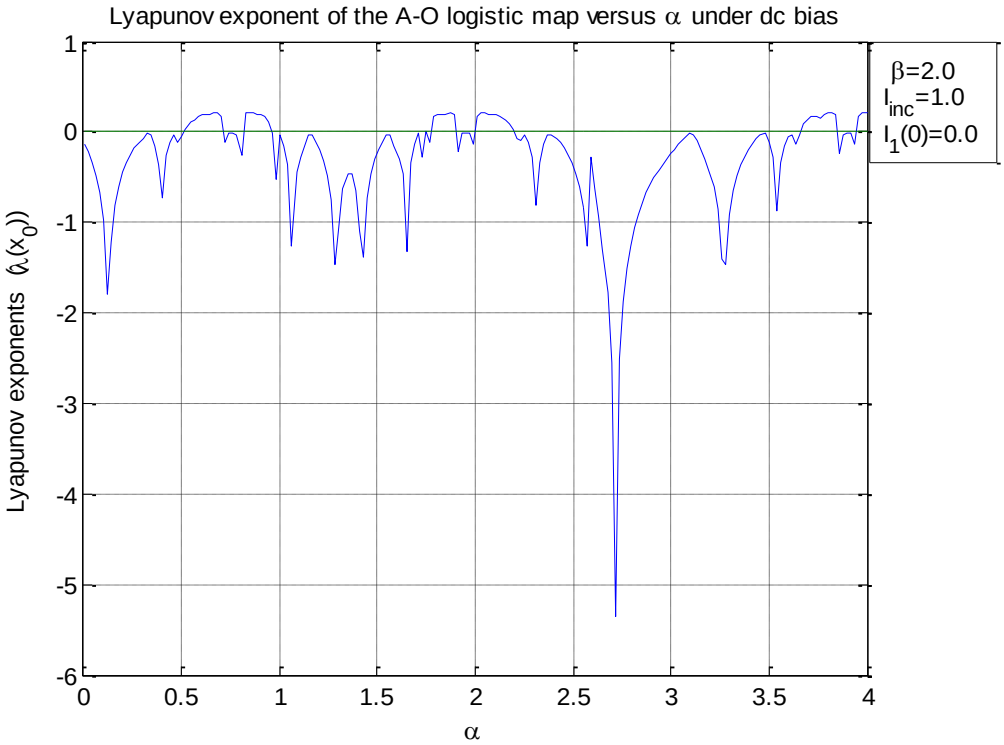

Fig.6. LE versus $\hat{\alpha}_0$ for $I_{inc} = 1$, $I_1(0) = 0$, and $\tilde{\beta} = 2$.

When $\tilde{\beta}$ is increased to 4, as shown in Fig.7, while keeping $I_{inc} = 1$ and $I_1(0) = 0$, we find that the chaotic bands have now increased noticeably. Thus, the LE is now positive over the bands of $\hat{\alpha}_0$ around the ranges listed in Table 1. Within these bands, however, there are narrow regions where the LE becomes negative, implying non-chaotic behavior. We will discuss the implications of these non-chaotic departures further later on. We need to point out here that in the chaotic modulation work that we have reported [5], a typical set of parameter values happens to be: $I_{inc} = 1$, $I_1(0) = 0$ and $\tilde{\beta} = 4$. The LE characteristics illustrated by Figs.(2-4) clearly indicate that with $\tilde{\beta} > 3$, we expect a relatively large range of chaotic $\hat{\alpha}_0$ values. This is important for our signal processing applications, since we need to ensure chaotic operation throughout the range of (ac + dc) $\hat{\alpha}_0$ values.

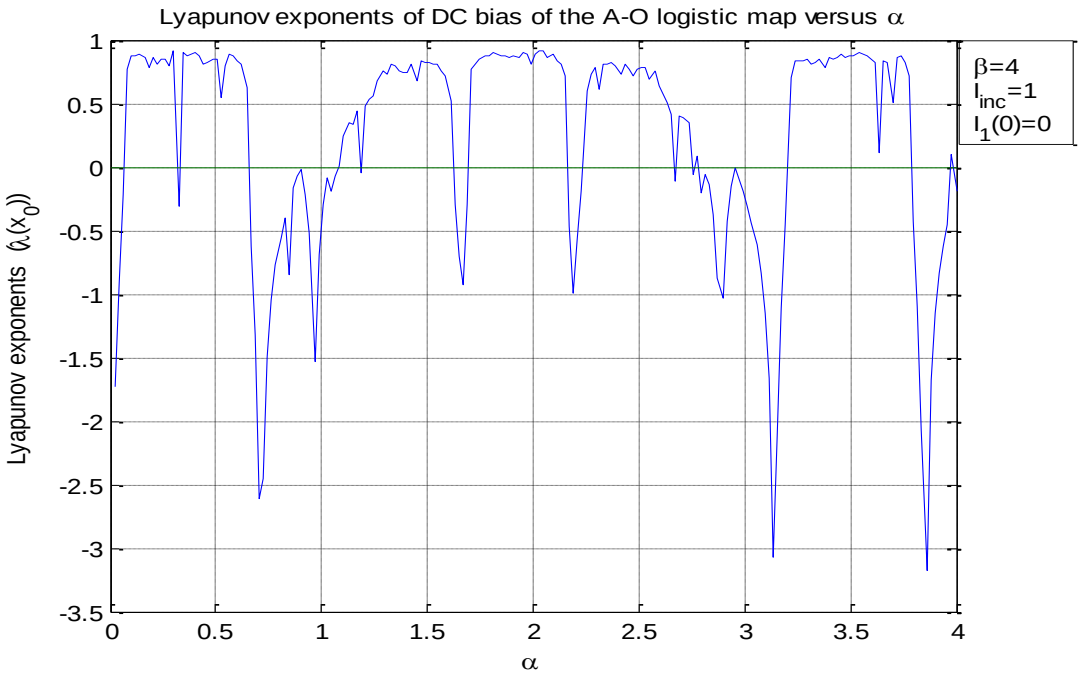

Fig.7: LE versus $\hat{\alpha}_0$ for I_{inc} = 1, I_1 (0) = 0, and $\tilde{\beta}$ = 4.

Overall, we observe that the sign of the LE depends critically on specific combinations of the four parameters, viz., $\hat{\alpha}_0$, $\tilde{\beta}$, $I_1(0)$, and I_{inc}. Therefore, there exists a great deal of sensitivity in terms of chaotic behavior over "pass" and "stop" bands of these parameters, especially $\hat{\alpha}_0$ and $\tilde{\beta}$. These issues will be examined in more detail later on, when we discuss the application of the LE to the signal encryption problem.

Table 1. Chaotic passbands and stopbands from numerical examination of LEs

Fixed Parameters			$\hat{\alpha}_0$	$\hat{\alpha}_0$	Bangaps
$\tilde{\beta}$	I_{inc}	$I_1(0)$	Passbands	Stopbands	$\Delta\alpha$
2	2	2	0.1 - 0.65	0.65 – 1.2	0.55
			1.2 – 1.55	1.55 – 1.65	0.1
			1.65 – 2.15	2.15 – 2.25	0.1
			2.25 – 2.7	2.7 – 3.2	0.5
			3.2 – 3.8	3.8 – 4.0	0.2
3	1	0	-	0 - 0.1	0.1
			0.1 – 0.65	0.65 – 0.7	0.05
			0.7 – 0.9	0.9 - 1	0.1
			1 – 1.6	1.6 – 3.25	1.65

			3.25 – 3.75	3.75 – 3.85	0.1
			3.85 - 4	-	-
3.5	1	0	-	0 -0.1	0.1
			0.1 - 0.3	0.3 – 0.35	0.05
			0.35 – 0.85	0.85 – 0.9	0.65
			0.9 – 1.2	1.2 – 1.85	0.65
			1.85 – 2.55	2.55 – 3.25	0.7
			3.25 – 3.45	3.45 – 3.5	0.05
			3.5 - 4	-	-
4	1	0	-	0 – 0.1	0.1
			0.1 – 0.65	0.65 – 1.3	0.65
			1.3 – 1.65	1.6 5– 1.85	0.2
			1.85 – 2.15	2.15 – 2.25	0.1
			2.25 – 2.6	2.6 – 3.25	0.65
			3.25 – 3.8	3.8 - 4	0.2
5	1	0	-	0 – 0.15	0.15
			0.15 – 0.85	0.85 – 0.95	0.1
			0.95 – 1.3	1.3 – 1.55	0.25
			1.55 – 1.9	1.9 - 2	0.1
			2 - 2.7	2.7 – 3.35	0.65
			3.35 - 4	-	-

2. EXAMINATION OF DYNAMICAL BEHAVIOR BASED ON BIFURCATION MAPS

In this section, we examine the dynamical behavior based on bifurcation maps of the AO cell with feedback in the Bragg regime, with the intent to compare the resulting dynamics with that predicted by the preceding Lyapunov theory. We first examine the second-order output intensity I_1 versus $\tilde{\beta}$ for fixed values of I_{inc} and $I_1(0)$ with $\hat{\alpha}_0$ held constant at 2.0. Two such results are shown in Figs.8 and 9. In Fig.8, $I_{inc} = I_1(0) = 0.55$, and $\hat{\alpha}_0 = 2$, we find that the first bifurcation starts at the value of $\tilde{\beta} = 1.8$, followed by a second-order bifurcation at $\tilde{\beta} = 3.2$, and chaotic behavior which starts to appear at $\tilde{\beta} = 3.5$. Furthermore, *uniform* or *steady state* chaos occurs only for $\tilde{\beta} > 3.7$. However, when the value of I_{inc} is set to 1, the initial condition $I_1(0)$ is set to 0, (this corresponds, incidentally, to the chaotic

encryption results reported elsewhere [5]), and $\hat{\alpha}_0$ = 2, the resulting bifurcation map shows considerable differences. This is shown in Fig.9. One notable change for this case is that the initial bifurcation, the second-order bifurcation, and the chaotic thresholds are all lower than the previous case (in other words, the map shifts to the left). Specifically, bifurcation now starts at $\tilde{\beta}$ = 1; second-order at 1.7 and *steady-state* chaotic behavior at about 2. Additionally, we observe another important dynamical feature in Fig.9. We find that within a broad chaotic "band", say from 2 to 2.75, there emerges a narrow "forbidden band" or "bandgap", where the output does not exhibit chaotic oscillations. Likewise, between 3.4 and 4, we find *steady-state* chaos. However, between 2.75 and 3.4, there is no chaos (even though there might be higher order multistability in this range). Note that these results are in complete agreement with those predicted by Lyapunov theory, as seen in Fig.4 previously.

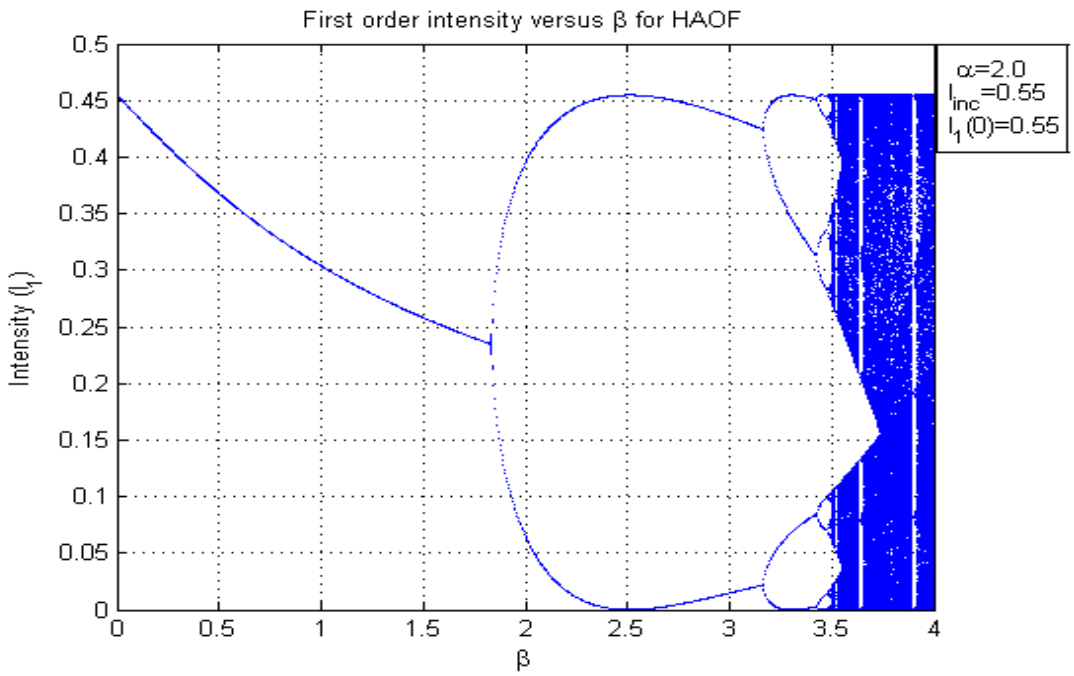

Fig.8. The bifurcation map of I_1 versus $\tilde{\beta}$ for fixed values of I_{inc} = 0.55, I_1 (0) = 0.55 and $\hat{\alpha}_0$ = 2.

From a closer examination of Figs. 4 and 9 corresponding to the LE parameter and the bifurcation map, we obsrve the following. The bifurcation map clearly predicts chaotic passbands and stopbands separated by bandgaps in the $\tilde{\beta}$ space. In comparing this finding with the LE plots discussed before, we recall that in the regions of $\tilde{\beta}$ where the LE became negative (indicating chaos), we have seen earlier how the LE undergoes negative transitions, indicating departure from chaos. Hence, both analyses predict very similar features. Examining Figs.4 and 9, we note that we can predict non-chaotic and chaotic behavior from each diagram via different interpretations. Thus, from Fig.4, we find that chaos happens in those windows where the LE becomes positive. Thus, we predict *chaotic* outputs for the case of $\hat{\alpha}_0$ = 2, I_{inc} = 1.0, and $I_1(0)$ = 0 over the $\tilde{\beta}$ windows (or passbands) 1.9-2.3, 2.4-2.75, and 3.2-4.0. Likewise, Fig.4 indicates *non-chaos* over the stopbands over 0-1.9, 2.3-2.4, and 2.75-3.2. From Fig.9, on the other hand, we define chaos as the regions of the I_1 vs. $\tilde{\beta}$ graph where we see *dense, steady oscillations* of the intensity in the $\tilde{\beta}$ space. By this definition, we find *chaotic* passbands in exactly the same regions as predicted by Fig.4. We note further that a stopband in Fig.9 is indicated by white *bandgaps* in the middle of an oscillatory waveform. One final note regarding the passbands has to do with the comparison of the last passbands in Figs.4 and 9, viz., in the range 3.2-4.0. In Fig.9, we find that the oscillations within this band do not uniformly sweep the vertical frame.

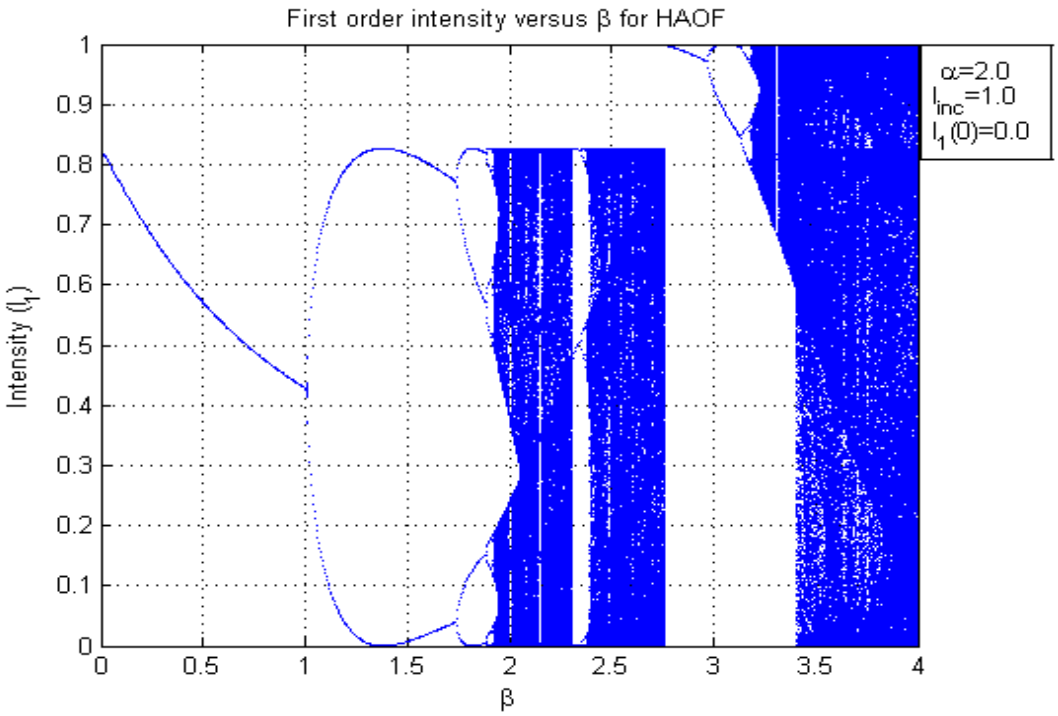

Fig.9. The bifurcation map of I_1 versus $\tilde{\beta}$ for fixed values of $I_{inc} = 1$, $I_1(0) = 0$ and $\hat{\alpha}_0 = 2$.

Returning to the same range in Fig.4, we find that the LE is actually positive in the entire range (thereby indicating chaos); however, in the region 3.2-3.3, there is a dip in the LE (i.e., the LE becomes smaller), thereby

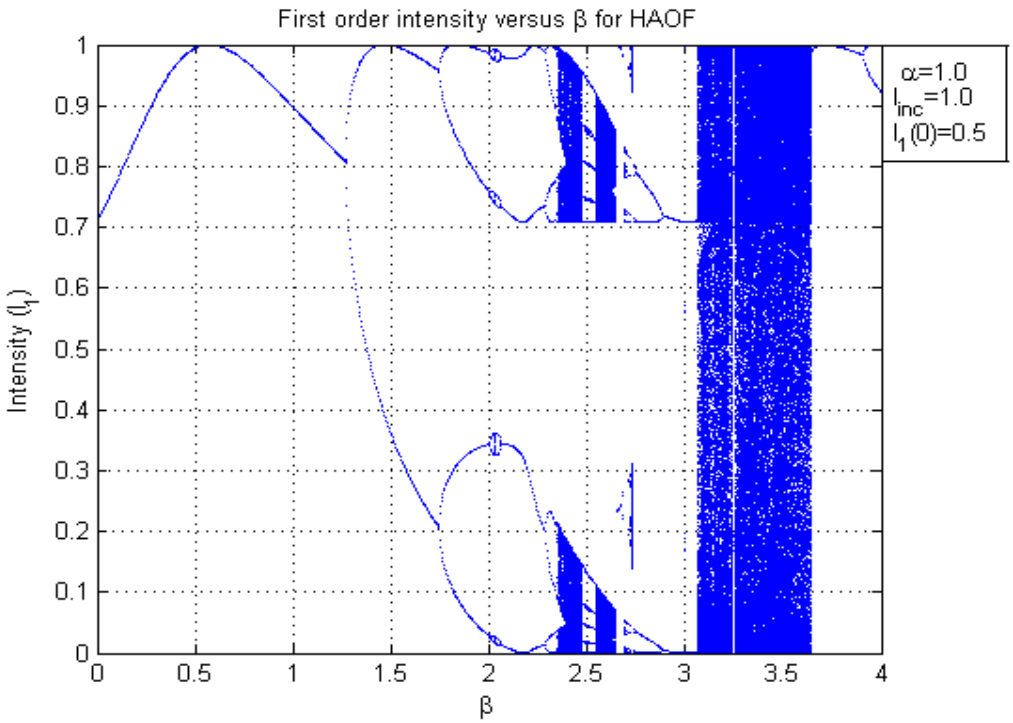

Fig.10. The bifurcation map of I_1 versus $\tilde{\beta}$ for fixed values of $I_{inc} = 1$, $I_1(0) = 0.5$ and $\hat{\alpha}_0 = 1$.

accounting for the non-uniformity in the oscillations in Fig.9 within the same band. In contrast, the dynamics of Fig.10 (with I_{inc} = 1, $I_1(0)$ = 0.5, and $\hat{\alpha}_0$ = 1), in the $\tilde{\beta}$ range (0-4), indicate a single chaotic passband, extending approximately from 3.1 through 3.6. In the region from 2.4-2.6, there appears to be some spurious, discontinuous oscillations, which we emphasize do not represent *steady state* chaos.

Figs.11-13 show bifurcation maps versus the bias parameter $\hat{\alpha}_0$. In these figures, we note certain fundamental differences from the bifurcations shown earlier versus $\tilde{\beta}$. From the figures, we once again see mono-, bi- and multistable regions created via the serial bifurcation effect. However, in this case, we observe a tendency (perhaps more pronounced) for the "bifurcation" to proceed both ways, i.e., a single branch undergoing doubling, as well as two branches combining into one. In addition, we find that the number of chaotic passbands in the $\hat{\alpha}_0$ space (for most typical fixed values of $\tilde{\beta}$) is consistently higher than was the case in the $\tilde{\beta}$ space. Thus, in Fig.11, with I_{inc} = 2, $I_1(0)$ = 2 , and $\tilde{\beta}$ = 2, we see five passbands separated by four stopbands. Details of these bands are summarized in Table 1.

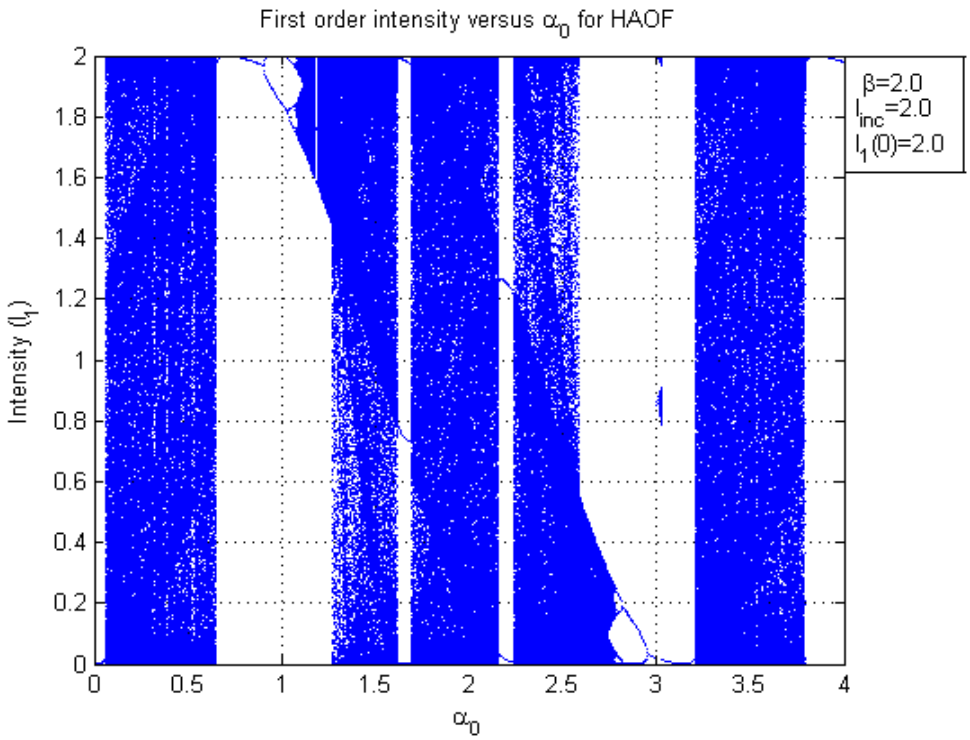

Fig.11. The bifurcation map of I_1 versus $\hat{\alpha}_0$ for fixed values of I_{inc} = 2, I_1 (0) = 2 and $\tilde{\beta}$ = 2.

In Fig.12, with I_{inc} = 1, $I_1(0)$ = 0 , and $\tilde{\beta}$ = 3, we find that the overall number of passbands is essentially two in this case, one running roughly from 0.1-1.6, and the other from 3.25-4. Within these two passbands, there are very narrow stopbands (of bandgaps within 0.1), where we expect the system to be non-chaotic. The two broad passbands are also separated by a wide bandgap from 1.6-3.25 (bandgap = 1.65), where there is no chaos. We note also that within the large stopband, there is an area with discontinuous oscillations in the intesnity (around 2.35-2.65), where the chaos is not steady-state.

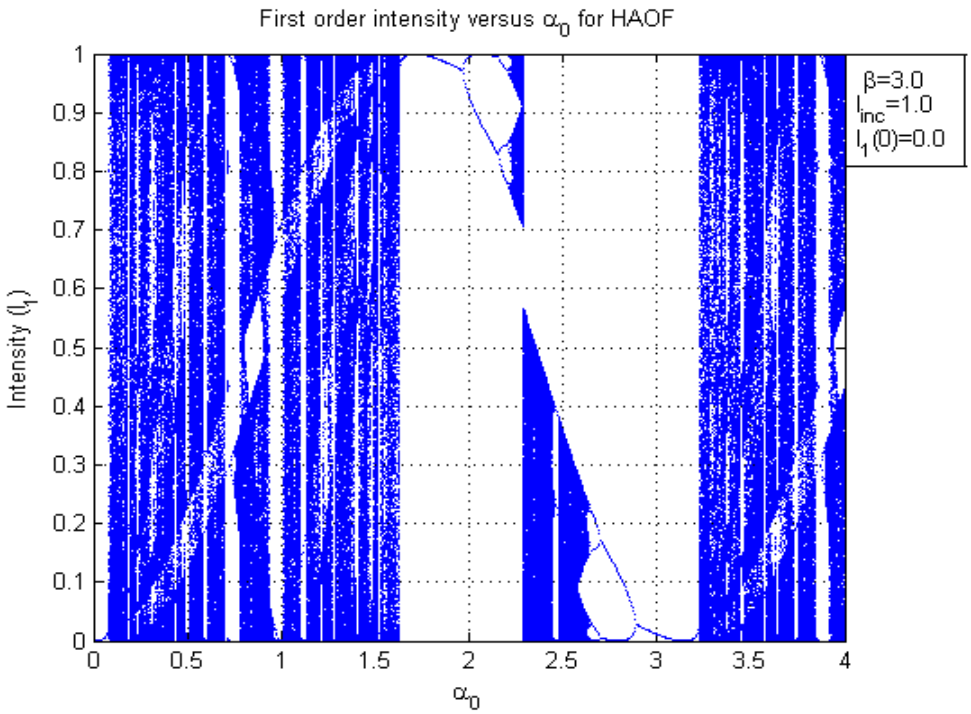

Fig.12. The bifurcation map of I_1 versus $\hat{\alpha}_0$ for fixed values of $I_{inc} = 1$, $I_1(0) = 0$ and $\tilde{\beta} = 3$.

Finally, in Fig.13, with $I_{inc} = 1$, $I_1(0) = 0$, and $\tilde{\beta} = 4$, we observe 5 very distinct and well-defined chaotic passbands (see Table 6.1), separated by two broad stopbands and two minor/narrow stopbands. Incidentally, some of the chaotic modulation work that we have recently reported [69] consisted of the same fixed parameter values as shown in Fig.13. From Table 1, we further remark that as the value of $\tilde{\beta}$ is increased above 3.0 (Fig.12), with $I_{inc} = 1$, $I_1(0) = 0$, the chaotic bands become progressively regular, continuous, and broader. Therefore, operating an AO feedback modulator within this range of parameters would offer greater leverage in terms of allowing larger ac amplitude variations, as well as ensuring reliable chaotic encryption within the entire passband. We will discuss the effect of discontinuous chaos and the resulting distortion on signal encryption elsewhere.

One particularly significant finding that we arrived at almost by serendipity was the following. Upon examining the bifurcation graphs of Figs.11 and 13, we find that *they look virtually identical*, even though the chosen values of the fixed parameters are quite different. In Fig.11, the parameters of interest are $I_{inc} = 2$, $I_1(0) = 2$, and $\tilde{\beta} = 2$. On the other hand, those corresponding to Fig.13 are $I_{inc} = 1$, $I_1(0) = 0$, and $\tilde{\beta} = 4$. Initially it seemed somewhat of a puzzle that large and identical chaotic bands (with identical stopbands) were emerging at feedback gains as different as 2 and 4, when in fact it has generally been assumed that one needs a relatively high $\tilde{\beta}$ value to achieve steady-state chaos. To further examine this apparent anomaly (i.e., might one get steady-state chaos at lower feedback gains, thereby reducing system power constraints?), we began to graphically look at fixed $\tilde{\beta} I_{inc}$ values, while varying the individual values of $\tilde{\beta}$ and I_{inc} . After a series of such plots (not shown here), it became clear that the nature of the chaotic behavior depended on the $\tilde{\beta} I_{inc}$ *product*, and not on their individual values, or the initial condition. This would then explain the identical nature of Figs.11 and 13, since the $\tilde{\beta} I_{inc}$ product for both happens to be 4. One might then rightly ask if there would be a preferred value of feedback gain to operate with (i.e. a lower or a higher value). Clearly, a *lower* feedback gain would require a *higher* incident optical power for the same chaotic characteristics, and *vice versa*.

Overall, this likely leads to a tradeoff issue; however, it certainly offers an option in that a loss of optical power might be compensated by increasing the feedback gain while maintaining the chaotic behavior.

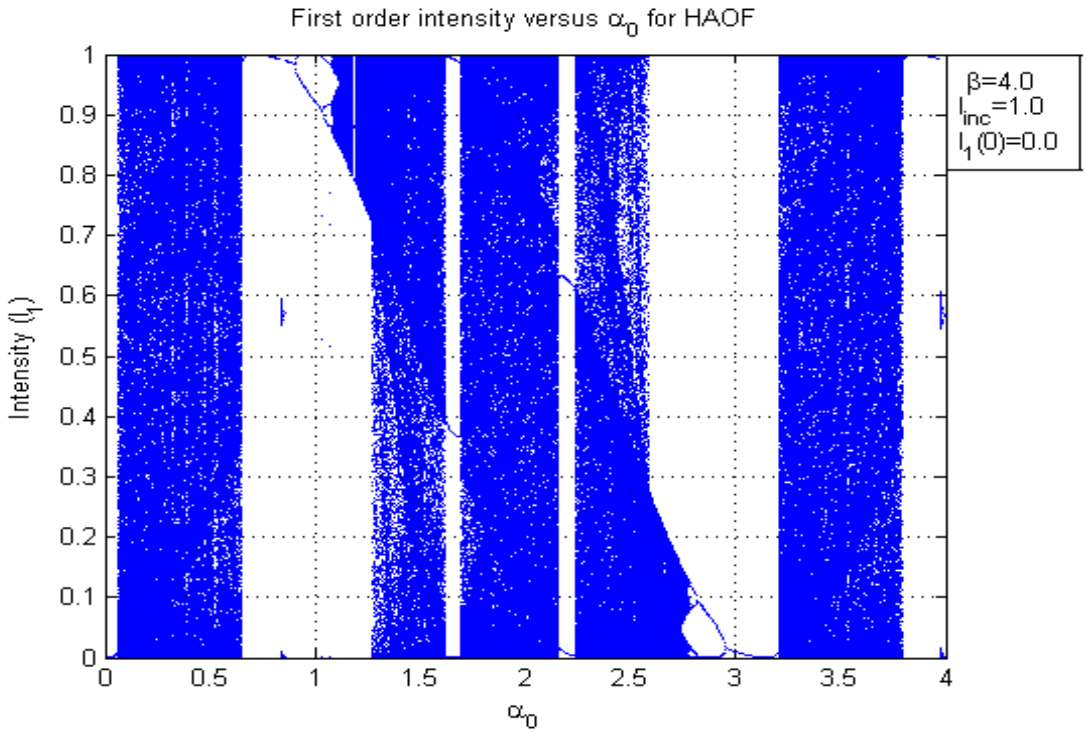

Fig.13. The bifurcation map of I_1 versus $\hat{\alpha}_0$ for fixed values of $I_{inc} = 1$, $I_1(0) = 0$ and $\tilde{\beta} = 4$.

3. CONCLUDING REMARKS AND FUTURE WORK

In conclusion, we remark that both the Lyapunov exponent analyses and the bifurcation maps offer viable means of understanding the conditions needed to achieve monostable, bistable, multistable and chaotic behavior in a complex, nonlinear closed-loop system such as HAOF. These findings have important implications in possible chaotic modulation and encryption applications, since the emergence of passbands and stopbands even within otherwise stable chaotic regimes shows that large signal dynamic ranges might not be allowable. Details of these findings are discussed in ref.[8].

In subsequent work, we will discuss the effect of the above properties of the HAOF in the chaotic regime in terms of practical signal encryption and recovery. Work on this is currently in progress.

REFERENCES

1. J. Albert, D. Vincent, and R. Tremblay, "Hybrid bistable optical device using an Acousto-optic waveguide modulator," Can. J. Phys. 59, 1251-1253 (1981).

2. J. Chrostowski and C. Delisle, "Bistable optical switching based on Bragg diffraction," Opt. Commun. 41, 71–74 (1982).

3. M.R. Chatterjee and J.-J. Huang, “Demonstration of acousto–optic bistability and chaos by direct nonlinear circuit modeling,” Appl. Opt. 31, 2506-2517 (1992).

4. A.K. Ghosh, P. Verma, S. Cheng, R.C. Huck, M.R. Chatterjee, and M. Al-Saedi, “Design of acousto-optic chaos based secure free-space optical communication links,” Proc. SPIE 7464, 74640L (2009).

5. M. Chatterjee, and M. A. Alsaedi, “Examination of chaotic signal encryption and recovery for secure communication using hybrid Acousto-optic feedback,” Opt. Eng. 50, 55002-1 – 055002-14 (2011).

6. A. K. Ghosh, and P. Verma, “Lyapunov exponent of chaos generated by acousto-optic modulators with feedback,” Opt.Eng. 50(1), 17005-1- 17005-5 (2010).

7. M. Chatterjee, M. A. Alsaedi, and A. K. Ghosh, “Performance measures in acousto-optic chaotic signal encryption system subject to parametric variations and additive noise,” Proc. SPIE, 7814, PP. 78140d1-15 (2010).

8. M. Al-Saedi, doctoral dissertation, University of Dayton, 2011.